Environmental Science & Technology

pubs.acs.org/est

Article

Model-Based Analysis of Reactive Transport Processes Governing Fluoride and Phosphate Release and Attenuation during Managed Aquifer Recharge

David Schafer, Jing Sun,* James Jamieson, Adam J. Siade, Olivier Atteia, and Henning Prommer*

Cite This: https://dx.doi.org/10.1021/acs.est.9b06972

Read Online

ACCESS | Metrics & More | Article Recommendations | Supporting Information

ABSTRACT: In water-scarce areas, the reclamation of wastewater through advanced water treatment and subsequent reinjection into depleted aquifers is an increasingly attractive water management option. However, such injection can trigger a range of water-sediment interactions which need to be well understood and quantified to ensure sustainable operations. In this study, reactive transport modeling was used to analyze and quantify the interacting hydrogeochemical processes controlling the mobilization of fluoride and phosphate during injection of highly treated recycled water into a siliciclastic aquifer. The reactive transport model explained the field-observed fluoride and phosphate transport behavior as a result of the incongruent dissolution of carbonate-rich fluorapatite where (i) a rapid proton exchange reaction primarily released fluoride and calcium, and (ii) equilibrium with a mineral-water interface layer of hydrated dibasic calcium phosphate released phosphate. The modeling results illustrated that net exchange of calcium on cation exchange sites in the sediments postbreakthrough of the injectant was responsible for incongruent mineral dissolution and the associated fluoride and phosphate release. Accordingly, amending calcium chloride into the injectant could potentially reduce fluoride and phosphate mobilization at the study site. Insights from this study are broadly applicable to understanding and preventing geogenic fluoride mobilization from fluoride-bearing apatite minerals in many other aquifers worldwide.

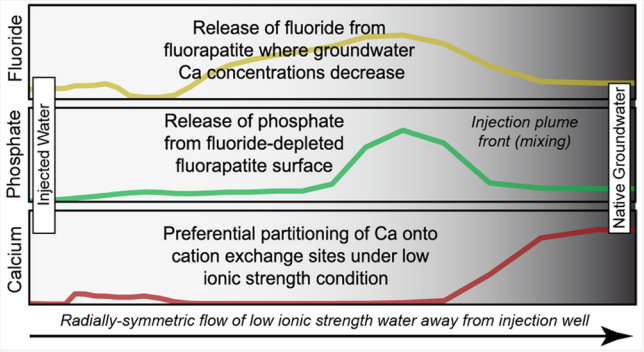

INTRODUCTION

Managed aquifer recharge (MAR) is an increasingly used water management option, particularly in water-scarce areas.[1−4] In many cases, MAR applications facilitate water banking, increase water recycling and enhance water security, while also providing passive treatment such as the removal of pathogens and the attenuation of organic micropollutants that may be present in the MAR source water.[2,5−7] However, in some cases, MAR can also trigger undesired geochemical processes in the recharged aquifer such as the mobilization of colloids and toxic metal(loid)s that may degrade groundwater quality.[3,8−15] The type and extent of these geochemical processes depend on the composition of the injectant (e.g., surface water, stormwater and recycled wastewater) and the hydrogeochemical characteristics of the target aquifer. For example, the injection of oxygenated water into anoxic aquifers often induces pyrite oxidation,[9,16,17] and sometimes associated with it, the mobilization of metal(loid)s such as arsenic.[11,18,19]

While fluoride intake at low levels is considered beneficial for humans and animals, excess fluoride in drinking water with concentrations >1.5 mg L^{-1} (79 μM) is detrimental to health as it causes dental and skeletal fluorosis.[20−23] Although much less attention has been paid to fluoride release in MAR systems compared to toxic metal(loid)s, fluoride release has been observed in multiple incidents during MAR, even where neither the native groundwater nor the injectant contains significant fluoride concentrations. For example, Gaus et al.[24] reported elevated fluoride concentrations during an aquifer storage and recovery (ASR) operation in a chalk aquifer due to fluorite dissolution. Stone et al.[25] also reported an ASR study where increased fluoride concentrations occurred during injection of fresh surface water into an alluvial aquifer. Brindha et al.[26] investigated the application of MAR to dilute high fluoride in weathered basement-rock aquifers and also discussed scenarios where increased fluoride release might occur. In our recent study, release of fluoride was also shown to occur during a field MAR experiment with highly treated recycled water.[27] Fluoride mobilization was accompanied by phosphate mobilization and hypothesized to be a result of the

Received: November 18, 2019
Revised: February 3, 2020
Accepted: February 4, 2020
Published: February 4, 2020

Table 1. Typical Initial (Native) Groundwater and Injectant Composition during the Field Injection Experiment

		native groundwater					
species	unit	120−138 mBGL	138−153 mBGL	153−171 mBGL	171−191 mBGL	191−225 mBGL	injectant
pH		6.6 ± 0.2	6.5 ± 0.2	6.6 ± 0.2	6.5 ± 0.1	6.7 ± 0.2	7.0 ± 0.2
temperature	°C	24.5 ± 0.8	24.9 ± 0.5	25.4 ± 0.4	25.9 ± 0.4	26.3 ± 0.4	26.0 ± 2.8
TDS	mg L^{-1}	380 ± 44	666 ± 55	916 ± 65	1047 ± 76	1111 ± 93	33.2 ± 10.9
DO	μM						518 ± 32
Cl	μM	4800 ± 1780	8600 ± 1860	14130 ± 1270	14530 ± 4570	17830 ± 2260	197 ± 59
Na	μM	3650 ± 478	7310 ± 522	11180 ± 1310	13400 ± 565	15570 ± 2130	448 ± 104
HCO_3	μM	1360 ± 229	1310 ± 148	1328 ± 229	1300 ± 180	1640 ± 361	228 ± 118
SO_4	μM	88 ± 20	406 ± 135	479 ± 88	573 ± 41	760 ± 135	1.5 ± 0.8
Si	μM	399 ± 57	483 ± 40	499 ± 52	549 ± 63	449 ± 28	15.0 ± 5.2
Ca	μM	599 ± 45	649 ± 20	649 ± 45	549 ± 20	649 ± 95	2.5 ± 0.0
Mg	μM	379 ± 49	823 ± 95	1152 ± 74	1280 ± 107	1320 ± 103	5.0 ± 1.2
K	μM	256 ± 20	332 ± 15	409 ± 20	435 ± 18	460 ± 41	26.0 ± 7.7
Fe	μM	91 ± 11	145 ± 16	143 ± 27	168 ± 16	125 ± 47	0.1 ± 0.0
Br	μM	6.8 ± 0.9	12.0 ± 0.8	16.0 ± 2.6	19.0 ± 3.8	21.0 ± 2.9	0.3 ± 0.0
N total	μM	14.0 ± 4.3	16.0 ± 3.6	16.0 ± 2.1	16.0 ± 2.1	15.0 ± 1.4	178 ± 59
F	μM	5.3 ± 2.6	6.8 ± 3.7	8.9 ± 3.7	10.0 ± 3.7	13.0 ± 2.1	6.3 ± 3.7
P total	μM	3.6 ± 1.3	5.2 ± 0.6	6.5 ± 1.0	9.4 ± 1.0	8.1 ± 2.3	0.6 ± 0.3
FRP[a]	μM	0.6 ± 0.6	0.3 ± 0.3	1.3 ± 1.6	0.6 ± 0.6	2.3 ± 3.2	0.3 ± 0.0
Mn	μM	0.9 ± 0.1	1.1 ± 0.1	0.9 ± 0.1	1.1 ± 0.1	1.3 ± 0.2	0.02 ± 0.00
B	μM	2.8 ± 0.9	1.9 ± 0.9	3.7 ± 2.8	2.8 ± 0.9	4.6 ± 3.7	9.3 ± 2.8
Al	μM	0.4 ± 0.1	0.4 ± 0.1	0.4 ± 0.1	0.4 ± 0.3	0.4 ± 0.1	0.2 ± 0.0

[a]FRP stands for filterable reactive phosphorus, which is assumed to represent phosphate.

dissolution of fluoride-bearing calcium-phosphate (apatite) minerals.

Fluoride-bearing apatite minerals, particularly carbonate-rich fluorapatite (CFA = $Ca_{10}(PO_4)_5(CO_3F)F_2$) and fluorapatite (FAP = $Ca_{10}(PO_4)_6F_2$), are ubiquitous accessory minerals in most igneous, metamorphic, and sedimentary rocks.[28,29] Previous experimental studies have demonstrated that FAP and CFA often contain a fluoride-depleted surface layer that controls mineral dissolution.[30−38] The mineral dissolution, and therefore release of fluoride and phosphate, occurs when the chemical equilibrium with this surface layer is disturbed, often in conjunction with removal of dissolved calcium in the system due to displacement of the native water with low-calcium water, cation exchange, and/or precipitation of calcium-bearing minerals.[39,40] To date, the risk of fluoride and phosphate mobilization by MAR with low ionic strength water has not been widely recognized. However, given the increasing importance of purified reclaimed waters or desalinated seawater as the source water for MAR and the number of MAR schemes that rely on aquifers containing fluoride-bearing apatite minerals,[41−43] potential water-sediment interactions need to be well understood and quantified to ensure sustainable operations. Reactive transport models (RTMs) that assist with untangling the many intertwined hydro-geochemical processes that control the fate of fluoride are fundamental to predict its long-term behavior in full-scale MAR schemes, where recycled water might be injected over several decades and large-scale groundwater quality changes are likely to occur.[44] RTMs are not only suitable to elucidate the contribution of individual geochemical processes and their interactions with groundwater flow and multispecies solute transport processes when used to interpret experimental data, but also to underpin the design of pretreatment system options that can mitigate the risk of mobilizing fluoride or other metal(oids).

The main objectives of this study were therefore to (i) identify and verify the mechanism(s) of fluoride and phosphate release during water injection in natural aquifers, and (ii) quantify the coupled flow, solute transport, and reactive processes. We employed a process-based reactive transport modeling approach to investigate the observed fluoride and phosphate release and attenuation patterns in a well-documented 4-year long field MAR experiment which injected highly treated, low ionic strength recycled water into a low-fluoride (<16 μM) sedimentary aquifer. On the basis of the identified reaction network, a series of model variants were constructed to elucidate the influences from different potential controlling factors. Finally, a mitigation strategy based on insights from modeling results is proposed to reduce the magnitude of fluoride and phosphate mobilization during MAR.

MATERIALS AND METHODS

Field Injection Experiment. The field injection experiment analyzed in this study was conducted at a site located ∼20 km north of metropolitan Perth, Western Australia (Figure S1 of the Supporting Information, SI).[16,44,45] During the experiment, highly treated recycled water was injected into the siliciclastic Leederville aquifer of the Perth Basin, through a single well screened between 124 and 224 m below ground level (mBGL). The injection interval is overlain by a carbonaceous confining layer and underlain by a silty clay layer (Figure S2). The aquifer section that was targeted by the injection consists of interbedded sand, silt and clay layers that were deposited in a near shore setting as tidally influenced distributary channel deposits, intertidal flat deposits, and tidal channel infills.[16,46] On the basis of X-ray diffraction (XRD) analysis, the sandy layers consisted of quartz (∼64%), feldspar (∼28%), and kaolinite (∼6%), whereas the clayey layers consisted of kaolinite (∼54%), feldspar (∼20%), and quartz (∼18%).[47] XRD also detected a number of trace minerals

https://dx.doi.org/10.1021/acs.est.9b06972
Environ. Sci. Technol. XXXX, XXX, XXX−XXX

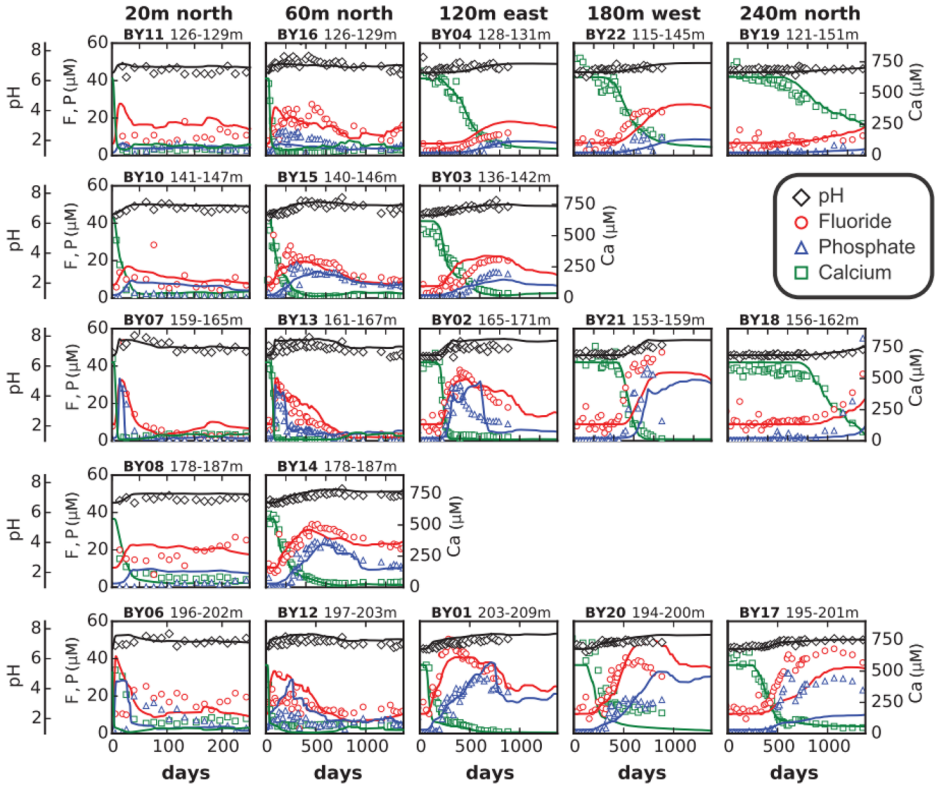

Figure 1. Observed and simulated groundwater pH, fluoride, phosphate, and calcium concentrations at different monitoring wells during the field injection experiment. See Figure S2 for monitoring well locations and screen depths. The depth of the screen intervals (in mBGL) is also noted next to the monitoring well name. Solid lines represent simulated results, whereas symbols represent observed concentrations (black diamonds = pH, red circles = fluoride, blue triangles = phosphate, and green squares = calcium).

including pyrite, lignite, chlorite, muscovite, biotite, and siderite. Additionally, CFA was identified as cement infill occurring within micaceous nodules found in a Leederville Formation core material at the field site.[27] The cation exchange capacity (CEC) of the Leederville sediments, as determined by ammonium chloride, varied between 1.5 and 6.9 cmol(+) kg^{-1} across the injection interval and was higher at fine grained lithologies. The native groundwater in the Leederville aquifer prior to the start of the injection was of Na−Cl to Na−Cl−HCO_3 type, anoxic, with total dissolved solids (TDS) ranging from ∼400 mg L^{-1} at the top of the injection interval to ∼1100 mg L^{-1} at the bottom (Table 1).[9]

In contrast to the native groundwater, the highly treated recycled water had high concentration of dissolved oxygen of 518 ± 32 μM (8.3 ± 0.5 mg L^{-1}) and low TDS of 33.2 ± 10.9 mg L^{-1} because of reverse osmosis treatment (Table 1). The highly treated recycled water also had lower concentrations of divalent cations (e.g., Ca^{2+} and Mg^{2+}) relative to monovalent cations, with a Na/Ca molar ratio of >180 ± 40, significantly higher than 15 ± 7 for the native groundwater and 45.6 for average seawater.[48] Over the 4-year period of the experiment, the highly treated recycled water was injected at an average daily injection rate of ∼2800 m^3 day^{-1} and a total of 3.9×10^6 m^3 was injected (Figure S3). The spreading of the injectant in the heterogeneous Leederville aquifer was monitored through an extensive groundwater sampling program. The monitoring network included 20 wells that were arranged in 5 multilevel well clusters located at a radial distance of 20, 60, 120, 180, and 240 meters from the injection well (Figures S1 and S2). Groundwater samples were collected from each of the monitoring wells at approximately monthly intervals, for which pH and temperature were measured in the field immediately after collection and the concentrations of a full suite of major and trace ions were determined during water quality analysis in the laboratory.[16,45] Each monitoring well was purged a minimum of three casing volumes prior to collection of groundwater samples. For each water quality sample, the groundwater was filtered using a 0.45 μm syringe filter into a polyethylene bottle, stored immediately on ice, and submitted for analysis on the same day of collection. Detailed descriptions of the sampling and analytical procedures are consistent with Water Corporation (2009).[45]

On the basis of the monitoring data, fluoride and phosphate release occurred immediately post breakthrough of the injectant (Figure 1).[27] Consistent with the observations from the field injection experiment, complementary laboratory batch experiments, performed with CFA-rich nodules recovered from the Leederville aquifer, also showed fluoride and phosphate release when an artificial groundwater matrix was progressively replaced by deionized water.[27] Similar batch experiments with sediment samples with low CFA content, on the other hand, showed no release of fluoride or phosphate (SI section S1). Therefore, the dissolution of CFA was hypothesized to be the most plausible explanation for the observed fluoride and phosphate release.[27] This hypothesis was further underpinned by additional geochemical modeling results that demonstrated that other than CFA, the native groundwater was undersaturated with respect to numerous other fluoride-bearing minerals such as fluorite.[27]

Numerical Modeling Approach and Tools. A coupled flow, solute/heat, and reactive transport model was previously developed to quantify the major redox and buffering processes

https://dx.doi.org/10.1021/acs.est.9b06972
Environ. Sci. Technol. XXXX, XXX, XXX−XXX

Table 2. Key Reactions Employed in the Final Calibrated Model and Associated Thermodynamic Constants That Affected Fluoride and Phosphate Mobilization and Attenuation[a]

CFA related reactions			starting log K	calibrated log K	ruv
$Ca_{9.75}Na_{0.25}(PO_4)_{5.37}(CO_3)_{0.55}F_{2.36}(OH)_{0.18} + 5.37H^+ + nH_2O \leftrightarrow \equiv Ca_{5.37}H_{5.37}(PO_4)_{5.37} \cdot nH_2O + 4.38Ca^{2+} + 0.25Na^+ + 0.55CO_3^{2-} + 2.36F^- + 0.18OH^-$				0.59	0.99
$CaHPO_4 \cdot H_2O \leftrightarrow Ca^{2+} + HPO_4^{2-} + H_2O$			−9.6[30]	−10.1	1.00
key cation exchange reactions	starting log K	calibrated log K		ruv	
$Na^+ + X^- \leftrightarrow NaX$	0[64]				
$H^+ + X^- \leftrightarrow HX$	5.08[16]				
$Ca^{2+} + 2X^- \leftrightarrow CaX_2$	0.8[64]				
$Mg^{2+} + 2X^- \leftrightarrow MgX_2$	0.6[64]				
key surface complexation reactions	starting log K	calibrated log K		ruv	
$\equiv GbOH + H^+ \leftrightarrow \equiv GbOH_2^+$	8.01[54]	8.01		0.59	
$\equiv GbOH \leftrightarrow \equiv GbO^- + H^+$	−11.57[54]	−11.66		3.6×10^{-06}	
$\equiv GbOH + PO_4^{3-} + 3H^+ \leftrightarrow \equiv GbH_2PO_4 + H_2O$	30[54]	31.00		0.23	
$\equiv GbOH + PO_4^{3-} + 2H^+ \leftrightarrow \equiv GbH_2PO_4^- + H_2O$	19.23[54]	19.23		0	
$\equiv GbOH + PO_4^{3-} + H^+ \leftrightarrow \equiv GbH_2PO_4^{2-} + H_2O$	14.8[54]	14.06		2.0×10^{-03}	
$\equiv GbOH + F^- + H^+ \leftrightarrow \equiv GbF + H_2O$	8.78[54]	9.78		5.9×10^{-03}	
$\equiv GbOH + F^- \leftrightarrow \equiv GbOHF^-$	2.88[54]	3.30		0.28	
$\equiv GbOH + 2F^- + H^+ \leftrightarrow \equiv GbF_2 + H_2O$	11.94[54]	11.94		1.2×10^{-06}	

[a]The complete set of reactions included in the model is provided in Table S4. The parameter values on cation exchange reactions were consistent with the values used in the previously published model[16] and not varied during model calibration in this study. In the table, X represents cation exchange sites; $\equiv$Gb represents composite surface complexation sites (initially based on gibbsite[54]); and ruv = relative uncertainty variance reduction[65] = $1 - \frac{\sigma_{ui}^2}{\sigma_i^2}$, where σ_i^2 and σ_{ui}^2 represent prior and posterior variances of parameter i (see SI Section S3 for further details).

during injection at the study site.[16,44,49] The previously published model was developed based on a comprehensive set of data that emerged from the hydrogeochemical characterization of the deep aquifer system through a combination of various geophysical and geochemical techniques, controlled laboratory-scale experiments, and the MAR field experiment. The model was previously shown to reproduce the observed heat and conservative solute data,[49] as well as the majority of the observed spatiotemporal geochemical responses to the injection.[16] The modeling results illustrated that the injection of oxic water into the reducing Leederville aquifer induced the oxidation of pyrite. Proton exchange with sediment cation exchange sites was identified to be the main pH buffering process preventing the acidification in the recharged Leederville aquifer.[16,44] As a first step for the present study, the previous model was extended to encompass the full 4-year period of the experiment and evaluated against the newly collected field observations. After minor modifications of hydraulic parameters affecting breakthrough profiles at more distal monitoring wells, the extended model provided a good description of the major ion and redox chemistry for the entire 4-year simulation period. This extended model was used in this study as the basis for evaluating various conceptual and numerical models describing the fate of fluoride and phosphate.

Flow Model Setup. MODFLOW[50] was used in this study for simulating groundwater flow. Compared to the flow that was induced by injection, regional groundwater flow at the field site was negligible (hydraulic gradient ~0.0006). Therefore, the groundwater flow conditions that persisted during the field injection experiment were, for simplicity and numerical efficiency, approximated by a 2-dimensional radial-symmetric model configuration (Figure S4). The model assumed confined groundwater conditions as the injection interval is overlain by a thick clay layer (Figure S2). The vertical model extent ranged from a depth of 97 to 225 mBGL, which comprised the entire injection interval (124−224 mBGL) and a small fraction of the overlying confining layer. The model comprised 76 layers in the vertical direction, which allowed for a detailed representation of aquifer bedding while assuming uniform hydrogeological conditions in the lateral direction. This assumption of laterally homogeneous layers may represent a source of model structural error, which would be problematic for other aquifer recharge configurations (e.g., multiple injection wells or recharge basins, multiple surrounding extraction wells, etc.) but based on Seibert et al.,[16,49] did not significantly impact the correctness of the model simulations over the monitored depth intervals and spatial scale in this field MAR experiment. The model comprised 41 columns in the lateral direction, and the grid discretization varied laterally between 2 m near the injection well and 100 m for the grid cell most distant from the injection well. A constant head boundary was placed at the outer edge of the model domain. The injection rates that were logged during the field experiment were discretized into daily time steps in the model to describe the sometimes highly variable flow conditions. Consistent with the duration of the field injection experiment, the total simulation period was 1378 days.

Reactive Transport Model Setup. PHT3D[51] was used for simulating reactive transport processes. The native groundwater and sediment characterization results were employed to define the initial conditions for the reactive transport model. The significant vertical geochemical heterogeneity in the Leederville aquifer was considered in the model by vertically separating the model into 6 distinct geochemical zones (Figure S4). These 6 zones were introduced to represent the increasing salinity and accordingly varying solute concentrations that occurred over the investigated depth interval prior to the start of the injection experiment. The selected zonation was directly adopted from our previously published model.[16] Within each of these geochemical zones, the initial water and sediment compositions were considered uniform. Regularly collected injectant water quality data were

https://dx.doi.org/10.1021/acs.est.9b06972
Environ. Sci. Technol. XXXX, XXX, XXX−XXX

considered in the model to describe the time-varying injectant water composition.

A reaction network consisting of a mixture of equilibrium and kinetically controlled chemical reactions was defined via the PHREEQC/PHT3D database. In the following, we mainly provide and discuss the details for the key reactions affecting the mobilization and attenuation of fluoride and phosphate (Table 2). All other reactions, notably pyrite oxidation and pH-buffering processes including proton exchange, remained consistent with the previously published model,[16,49] and the relevant reactions, stoichiometries, and equilibrium constants are provided in Table S4. Since the average measured temperature of the native groundwater was 25.7 ± 1.6 °C, equilibrium constants at 25 °C were adopted for all reactions.

With CFA being identified as the most likely source of the released fluoride and phosphate in the Leederville aquifer,[27] CFA dissolution was included in the reaction network. On the basis of microprobe analyses on the CFA-rich nodules collected from the Leederville aquifer which were interpreted using the "francolite" model of McClellan,[52] $Ca^{9.75}Na^{0.25}(PO^4)^{5.37}(CO^3)^{0.55}F^{2.36}(OH)^{0.18}$ was found to be the representative formula for CFA in the recharged aquifer.[27] On the basis of previous experimental studies with CFA[36] and the closely related FAP,[30−33] the dissolution of fluoride-bearing apatite minerals often involves an initial rapid proton exchange reaction whereby H^+ is adsorbed onto the mineral surface, triggering the preferential removal of calcium, fluoride, and carbonate. On the basis of Chaïrat et al.,[31] this rapid incongruent (nonstoichiometric) dissolution process can be approximated as follows:

$$Ca_{9.75}Na_{0.25}(PO_4)5.37(CO_3)_{0.55}F_{2.36}(OH)_{0.18} + 5.37H^+ + nH_2O \leftrightarrow \equiv Ca_{5.37}H_{5.37}(PO_4)_{5.37}\cdot nH_2O + 4.38Ca^{2+} + 0.25Na^+ + 0.55CO_3^{2-} + 2.36F^- + 0.18OH^- \quad (1)$$

The rapid proton exchange reaction (reaction 1) was incorporated into the PHREEQC/PHT3D database as an equilibrium-controlled exchange reaction using the Gaines-Thomas convention (full details are provided in SI section S2). The exchange selectivity coefficient for this reaction was included as an adjustable parameter during model calibration. The modeled exchange reaction (reaction 1) serves as a surrogate for the incongruent dissolution process, resulting in the production of a surface layer with a composition equivalent to hydrated dibasic calcium phosphate (DCPsurface: $\equiv Ca_{5.37}H_{5.37}(PO_4)_{5.37}\cdot nH_2O$ with ≡ representing a surface layer instead of a pure mineral).[30−33,36] In conjunction with Reaction 1, dissolved calcium and phosphate concentrations are also affected by equilibrium with DCPsurface:

$$\equiv Ca_{5.37}H_{5.37}(PO_4)_{5.37}\cdot nH_2O \leftrightarrow 5.37Ca^{2+} + 5.37HPO_4^{2-} + nH_2O \quad (2)$$

The solubility product (log $K_{SP}^{25\ °C}$) of DCPsurface per unit on FAP was previously determined to be −9.6 ± 0.6 by Chaïrat et al.[30] Therefore, DCPsurface was assumed to be more stable than DCP as a pure mineral phase (log $K_{SP}^{25\ °C}$ = −6.7).[53] DCPsurface was defined in the PHREEQC/PHT3D database as an equilibrium mineral phase. The previously reported solubility product for DCPsurface on FAP (i.e., −9.6) was adopted as the initial estimate of the solubility product for DCPsurface in the Leederville aquifer.[30] It was then allowed to deviate during model calibration. Potential dissolution/precipitation reactions of calcite, dolomite, ankerite, vivianite, fluorite, gypsum, and various other calcium phosphate minerals were also evaluated but found unlikely to be important in this study.

To account for the potential for cation exchange reactions to affect groundwater quality evolution during the field injection experiment, an exchanger site (X) was implemented in the model. The equilibrium constants for proton exchange and other cation exchange reactions were consistent with the values used in the previously published model,[16] and were not varied during model calibration in this study. To account for the competitive adsorption and desorption reactions that may have affected fluoride and phosphate mobility during the experiment, a surface complexation model (SCM) was also included in the reaction network. Sorption was represented by a single site SCM based on the generalized diffuse layer model for gibbsite ($Al(OH)_3$) by Karamalidis and Dzombak.[54] The surface sites on gibbsite were selected as the representative sites because (i) the reducing Leederville aquifer contained high aluminum content (9.5 ± 5.7 wt % Al as Al_2O_3);[47] and (ii) based on the calculated saturation index, the Leederville aquifer was also found to be in equilibrium with microcrystalline gibbsite (SI = −0.05 ± 0.24).[55] The initial estimates for the intrinsic equilibrium constants for the surface complexation reactions in the Leederville aquifer were assumed to be equal to those for gibbsite, based on Karamalidis and Dzombak for an ionic strength (I) of 0.001 M,[54] which corresponded approximately to the ionic strength of the injectant. Where intrinsic equilibrium constants were not available for I = 0.001 M, equilibrium constants determined for higher ionic strength were adopted as initial estimates in the SCM.

Model Calibration Procedure. For the reactive transport model developed in the present study, the adjustable parameters (Tables 2 and S4) included (i) the initial concentrations of CFA, DCPsurface, cation exchange sites, and composite surface complexation sites in the Leederville sediments, (ii) the selectivity coefficient for the CFA exchange reaction (reaction 1), (iii) the equilibrium solubility product for DCPsurface (reaction 2), and (iv) some of the equilibrium constants for the surface complexation reactions. The parameters were initially selected based on literature values and sediment characterization results, where available, then further adjusted to minimize the sum of the squared residuals between model results and field observations while still adhering to the literature values as closely as possible. Following an initial manual trial-and-error step, the parameters were further refined during automatic calibration using PEST++.[56] The observation data used to constrain the automatic calibration consisted of dissolved fluoride, phosphate (measured as filterable reactive phosphorus, FRP), calcium, and pH measurements from all the monitoring locations over the 4-year experimental period. The procedure of observation weight assignment was adopted from Sun et al.[57] Additional details of the model calibration procedure are provided in the SI section S3.

RESULTS AND DISCUSSION

Observed Breakthrough Behavior of Fluoride and Phosphate. During the field injection experiment, pulses of elevated groundwater fluoride (12−58 μM) and phosphate (3.9−55 μM) concentrations were observed at all monitoring locations (Figure 1). Although fluoride and phosphate were released over the entire depth of the injection interval, a slight

https://dx.doi.org/10.1021/acs.est.9b06972
Environ. Sci. Technol. XXXX, XXX, XXX−XXX

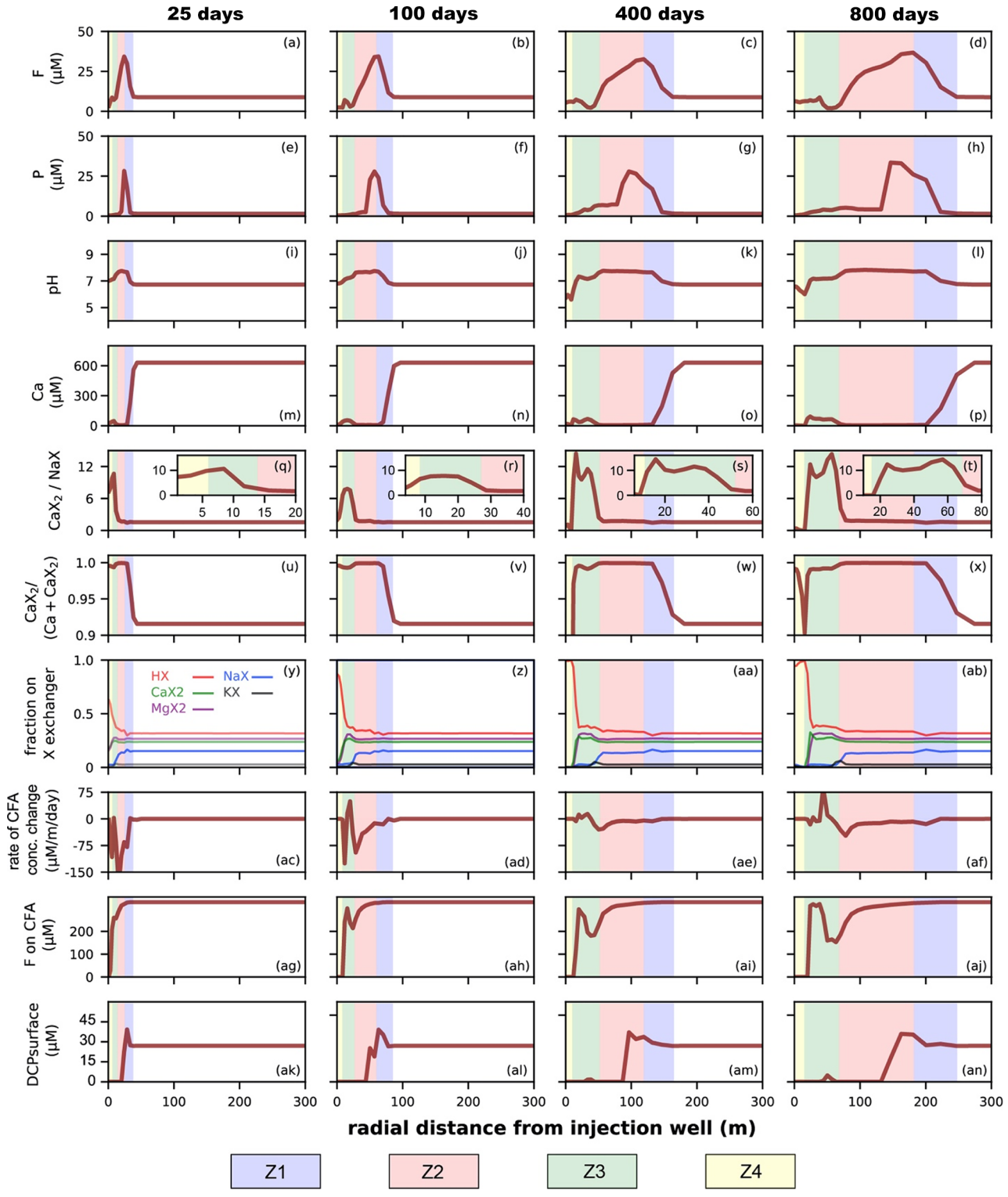

Figure 2. Simulated length profiles at a depth interval of 161−162.4 mBGL in the central section of the recharged Leederville aquifer at selected times after the injection started. Blue, red, green, and yellow shading in the background mark geochemical zones Z1−Z4, respectively.

increase in released concentrations with depth was observed. The fluoride and phosphate release occurred upon injectant breakthrough in association with the sharp declines in groundwater calcium concentrations caused by the low-ionic-strength and thus low-calcium injectant (Figure 1 and Table 1). The pulses of elevated fluoride and phosphate concentrations also coincided with a slight increase in pH. During injectant breakthrough, groundwater fluoride concentrations tended to rise marginally earlier than phosphate concentrations. The observed pulses broadened with increasing radial distance from the injection well. However, neither peak fluoride nor phosphate concentrations increased appreciably beyond 60 m from the injection well (Figure 1).

Observed and Simulated Spatiotemporal Evolution of Geochemical Zonation. On the basis of previous work[16] and the model-based analysis of the observations in this study,

https://dx.doi.org/10.1021/acs.est.9b06972
Environ. Sci. Technol. XXXX, XXX, XXX−XXX

pyrite oxidation, pH buffering, and net exchange of calcium onto the sediment cation exchange sites were identified as the most important reactive processes affecting the hydrochemistry in the recharged Leederville aquifer. These geochemical reactions, coupled to the physical solute transport processes, can explain the observed breakthrough behavior of the major ions, pH, redox-sensitive trace species, fluoride, and phosphate at the monitoring wells. The breakthrough behavior of many major ions and redox species were already matched and quantified by our previous model simulations, as discussed in detail in Seibert et al.[16] In this study, the reactive transport model was further refined to provide insights into the temporal evolution of the geochemical zonation as a prerequisite for the subsequent identification of the critical controls for the fate of fluoride and phosphate. The results of the calibrated reactive transport model show the formation and dynamic progression of four distinct geochemical zones along the radial direction. Starting from the injection plume front and moving inward to the injection well, the four zones Z1−Z4 are highlighted by respective shadings in Figure 2.

At the injection plume front, the transition between the native and the injection-impacted groundwater compositions marks the geochemical zone Z1 (blue shading). Within Z1, the concentrations of most of the major ions sharply decrease, because the highly treated, low ionic strength recycled water actively displaces the native groundwater. For example, dissolved calcium concentration decreased from the native groundwater concentration of ∼630 μM to only 3−7 μM within Z1 (Figure 2m−p). At the injection plume front, the Ca/Na molar ratio on sediment exchange sites, denoted as CaX_2/NaX, is ∼1.6, which is similar to the ratio occurring in the native Leederville aquifer, indicating that minimal cation exchange occurred in Z1 (Figure 2q−t).

Upstream of the active transition zone Z1, a second zone Z2 develops (red shading). This zone is characterized by the presence of consistently low ionic strength groundwater as a result of the displacement of the native groundwater. In Z2, dissolved calcium concentrations remained low at ∼3−7 μM (Figure 2m−p) while the pH increased slightly (Figure 2i−l). The proportion of calcium that partitions onto cation exchange sites is high (∼99.8%) (Figure 2u−x), and the CaX_2/NaX ratio is increased by ∼25% to approximately 2.0 (Figure 2q−t). This indicates that calcium was gradually exchanged for sodium on the sediments. The extent of Z2 became wider over time, and its width increased to over 100 m after 800 days from the start of injection.

Further toward the injection well, zone Z3 (green shading) is characterized by somewhat elevated calcium concentrations (50−70 μM), an order of magnitude higher than that of Z2, and a cation exchange site occupancy that significantly differs from the composition that was originally in equilibrium with the native groundwater. This zone shows distinctly increased CaX_2/NaX ratios on the cation exchange sites (∼10−15, Figure 2q−t), as sodium was successively displaced from the exchanger, mostly by protons (denoted as HX, Figure 2y−ab). The protons were generated near the injection well due to pyrite oxidation (and the associated iron(III) hydrolysis) and advected into Z3. The uptake of protons on the sediment exchange sites in Z3, referred to as proton buffering, effectively buffered the acidity and maintained the circumneutral pH of the recharged Leederville aquifer.[16] Due to the higher selectivity for higher valence ions under the induced low ionic strength conditions, the fraction of calcium and magnesium on the cation exchange sites did not change in Z3 (Figure 2y−ab).

The innermost zone Z4 (yellow shading) is the zone where the oxic injectant triggers pyrite oxidation and, hence, acid generation.[9,16,58] The extent of this zone remains limited to <15 m around the injection well, with dissolved oxygen becoming rapidly depleted. Inside Z4, all major cations were almost entirely displaced from the exchange sites by protons (Figure 2y-ab). Consequently, the buffering capacity within this zone was rapidly exhausted.

Simulated Fluoride Transport Behavior. The simulated fluoride breakthrough curves reproduced the observed fluoride breakthrough behavior at most of the monitoring wells (Figure 1). Both observed and simulated fluoride breakthrough concentrations are the result of a combination solute transport and reaction processes. The simulation of the flow and physical transport processes already accounts for many of the hydrogeological complexities such as the highly variable flow rates and the strong vertical heterogeneity. Nevertheless, some of the deviations between simulated and observed concentrations were most likely induced by simplifications (e.g., laterally homogeneous hydrogeological conditions) and structural errors in the geological model and the associated inaccuracies in the simulated physical transport behavior (e.g., for BY04 and BY20).[58] In addition to physical transport, the two reactive processes that were hypothesized in our conceptual and numerical models to regulate spatiotemporal groundwater fluoride concentrations were (i) the CFA dissolution/precipitation reaction (reaction 1) and (ii) fluoride adsorption on the sediment surfaces. The modeling results suggested that the latter process had no measurable impact on the fluoride transport behavior (i.e., the fluoride breakthrough curves were found to be almost identical with or without fluoride surface complexion reactions, Figure S5), and fluoride water-sediment partitioning was primarily controlled by CFA equilibria. Radial profiles of dissolved fluoride show that the front end of the fluoride plume is located within geochemical zone Z1, i.e., within the active transition zone close to the injectant plume front; and the back end of the fluoride plume is located near the interface between Z2 and Z3 (Figure 2).

The profiles of the integrated rates of CFA concentration change (Figure 2ac−af, negative values indicate CFA dissolution, positive values indicate precipitation) show that CFA dissolution initially occurs in Z4 (Figure 2ac). However, after 100 days, the majority of the release occurs within Z2 and in particular near the Z2/Z3 interface (Figure 2ad−af). With the Z2/Z3 interface being identified as the main "source zone" for fluoride release, this implies that the elevated groundwater fluoride concentrations in Z1 and Z2 (i.e., beyond the Z2/Z3 interface) resulted from the combination of active local release at larger radial distances and, at some locations more importantly, the advective-dispersive physical transport of the already released fluoride. Interestingly, the calculated rates of CFA concentration change also suggest that specifically within Z3, the precipitation of CFA occurs, which locally reduces dissolved fluoride concentrations. The spatial CFA dissolution patterns are also demonstrated by the simulated fluoride concentrations on CFA (Figure 2ag−aj, concentrations below the initial concentration indicate that fluoride release has occurred). The simulated concentrations along the profile illustrate that a complete depletion of fluoride on CFA has occurred within Z4, i.e., in the direct proximity of the injection well. Fluoride release within Z1 and Z2, i.e., near and just

https://dx.doi.org/10.1021/acs.est.9b06972
Environ. Sci. Technol. XXXX, XXX, XXX−XXX

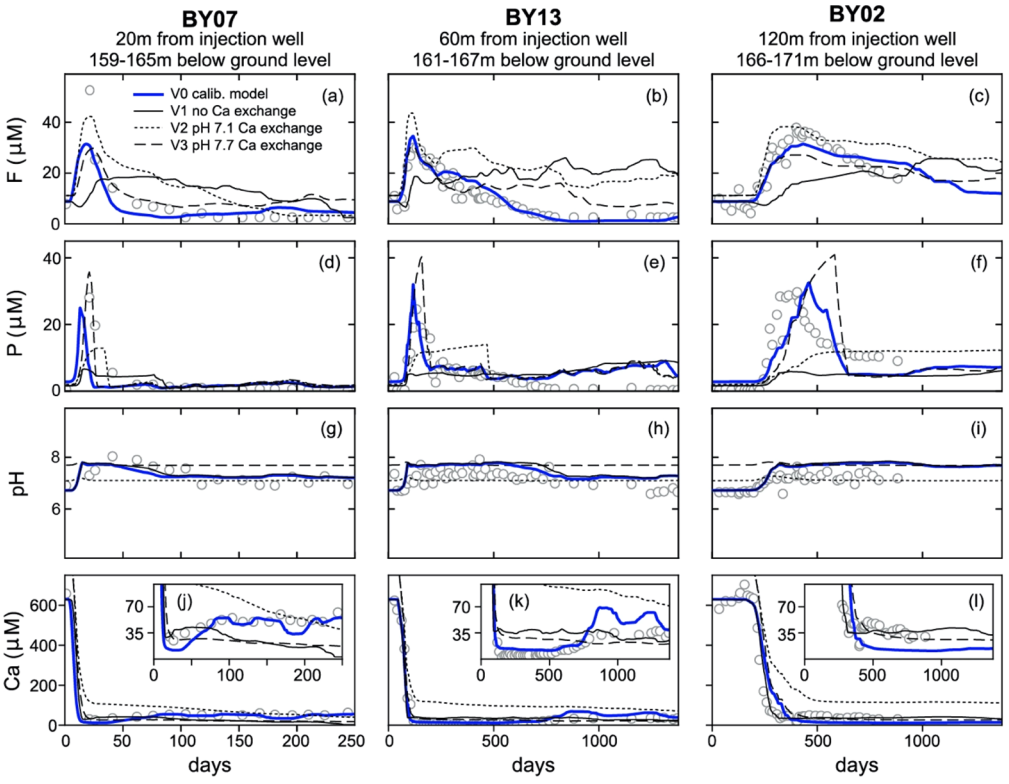

Figure 3. Breakthrough curves at selected monitoring wells from the central section of the recharged Leederville aquifer for different model variants—V0: final calibrated model, V1: no calcium exchange reaction, and V2: pH 7.1 and V3: pH 7.7. More details on model variants are given in SI section S5. Solid and dashed lines are simulation results, and symbols represent the observations.

behind the injectant plume front is generally negligible, except for shortly after the start of the injection. This is because the injectant that is being transported behind the plume front has quickly reached its new equilibrium with CFA locally within the aquifer. Overall, these model-based findings suggest that although CFA dissolution occurred to some extent due to the injection, such CFA dissolution still would not lead to detrimental level of fluoride contamination in the Leederville aquifer.

Key Controls on the Release and Attenuation of Fluoride. Among the many interrelated processes that occurred during the field injection experiment, the processes affecting the fate of calcium and pH played a key role in the release and attenuation of fluoride, as they most significantly disturbed the prevailing geochemical equilibrium between the native groundwater and CFA (reaction 1). Cation exchange and its impact on dissolved calcium concentrations were the major controls for the times and locations of elevated fluoride concentrations in this field injection experiment. This finding can be illustrated by a variant of the final calibrated model, in which the calcium exchange reaction with the sediment exchange sites was omitted from the reaction network, while an artificial ("ghost") calcium species was added in the model at a concentration that was equivalent to the calcium concentration in the injectant to ensure that in this model variant, V1, other than calcium itself being excluded, cation exchange processes involving all the other cations could still operate in the same way as in the final calibrated model, V0 (see SI section S4 for further details on the model variants). While V0 closely reproduces the breakthrough behavior of pH, calcium, and fluoride, model variant V1 shows significantly retarded release of fluoride (Figure 3a–c). These modeling results highlight that the net exchange of calcium onto sediment exchange sites significantly regulated dissolved calcium concentrations, and consequently, CFA solubility.

The effect of pH on fluoride release was investigated by two additional model variants, V2 and V3. In these two model variants, the pH of the injectant was artificially buffered to the lowest (pH 7.1, V2) and highest (pH 7.7, V3) pH values that were observed within the injection impacted aquifer zones, respectively (Figure 3a–c, g–i), while calcium exchange reaction was included in these variants in the same way with the final calibrated model (V0). On the basis of comparisons between V0, V2, and V3, the magnitude of fluoride release increases as pH decreases (Figure 3a–c).

To further illustrate the influence of groundwater calcium concentrations and pH, we considered a simplified batch system where dissolved fluoride is in equilibrium with CFA, and computed fluoride concentrations under varying calcium concentrations, solution pH, as well as the amount of CFA in the native aquifer (see SI section S5 for the detailed calculations). In this batch system, while dissolved calcium concentrations increased from 1 to 10 μM, dissolved fluoride concentrations decreased more than 10-fold (Figure 4). The model-simulated groundwater fluoride concentrations in Z2 and Z3 were taken from the final calibrated model (V0) at 800 days and also plotted on Figure 4. Elevated groundwater fluoride concentrations in Z2 (pH 7.7) correspond to low calcium concentrations, while substantially lower groundwater fluoride concentrations in Z3 (pH 7.1) are associated with elevated calcium concentrations. With a 0.6 unit increase in the solution pH, dissolved fluoride concentrations decrease over 1 order of magnitude. Alternatively, the concentration of CFA in the native aquifer plays a smaller role on dissolved fluoride

https://dx.doi.org/10.1021/acs.est.9b06972
Environ. Sci. Technol. XXXX, XXX, XXX−XXX

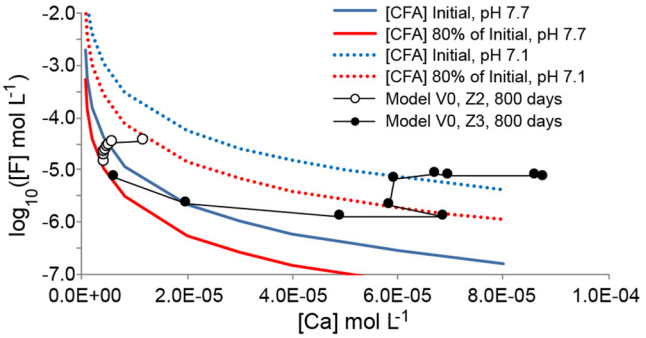

Figure 4. Dissolved fluoride concentrations (in log scale) as a function of dissolved calcium concentration where the aqueous solution is in equilibrium with CFA in a batch system. Solid lines represent the case where the pH is 7.7, while dotted lines represent the case where the pH is 7.1. Blue lines present the case that the initial CFA concentration is set equal to average initial concentration in the reactive transport model, and red lines indicate the case where 20% reduction of the initial CFA concentration are used. Circles represents the concentrations computed by the reactive transport model for the geochemical zones Z2 and Z3 for a simulation time of 800 days. Further details on the calculations are provided in SI section S5.

concentrations, as shown by the cases where a 20% reduction in initial CFA concentration lead to ~3 times lower dissolved fluoride concentrations. These results show that the elevated fluoride concentrations occurring in a narrow range of chemical composition (low calcium concentration and slightly alkaline pH) are related to the CFA exchange equilibrium constant (reaction 1) and local hydrochemistry. A small variation of the chemical compositions from the Z2/Z3 boundary and across the Z2 zone explain the observed broad peak of fluoride.

Key Controls on the Release and Attenuation of Phosphate. Similar to the case of fluoride, the release of phosphate was also initiated by the injection-induced disturbance of the geochemical equilibrium that originally persisted between the native groundwater and the DCPsurface (Reaction 2). Accordingly, the transport of calcium and its exchange reaction with the sediment exchange sites play an equally important role on controlling the times and locations of phosphate release. The longitudinal profiles show that the initially prevailing DCPsurface dissolves completely in conjunction with the decrease of calcium concentration during breakthrough of the injectant in Z1 (Figure 2ak–an). A similar phosphate release process, under low ionic strength conditions, that was observed in this MAR study in fact also occurs in many other environmental systems. For example, when low ionic strength rainwater infiltrates soil systems, phosphate release to soil porewater sometimes occurs because divalent calcium ions preferentially partition onto soil cation exchange sites and trigger the dissolution of otherwise insoluble apatite minerals.[59]

Although the fate of phosphate in aquifers is often regulated by surface adsorption,[19,60] similar to the case of fluoride, the mobility of phosphate in this field injection experiment does not appear to be affected by adsorption on the sediments. The impact of the sorption reactions is illustrated by the comparison of the simulation results of the final calibrated model, V0, and model variant, V4, in which the SCM was omitted from the model framework (Figure S5). The results of model variant V4, without the surface complexation reactions, show almost identical phosphate breakthrough behavior with V0. The fact that the model could reproduce the observations on phosphate without a SCM suggests that phosphate has a low affinity for sediment surfaces in the Leederville aquifer. This is possibly because the pH sorption edge for phosphate on the sediments is below 7.1, which is consistent with gibbsite and some clay minerals abundant in the Leederville aquifer.[54,61]

IMPLICATIONS

In this study, the model-based interpretation of a field MAR experiment that injected low ionic strength recycled water into a CFA-bearing aquifer has isolated which of the multitude of coupled physical and geochemical processes exert a key control on the elevated fluoride concentrations in the groundwater. Our process-based reactive transport model has highlighted the important role of cation exchange reactions on dissolved calcium concentrations and the associated fluoride and phosphate release. The insights obtained from the model suggest that the majority of the fluoride and phosphate release occurred in the early stages of the injection, and that the release would most likely not lead to uncontrollably high groundwater fluoride concentrations in the recharged aquifer. Therefore, there is a low risk that large-scale application of MAR could create a concerning level of fluoride contamination at the study site.

Furthermore, on the basis of the conceptual and numerical model framework that was established in this study, predictive modeling can now be employed to assess possible mitigation strategies that would allow to ensure water quality in this MAR system. For example, the model can be used to predict whether undesirable water-sediment interactions could be suppressed

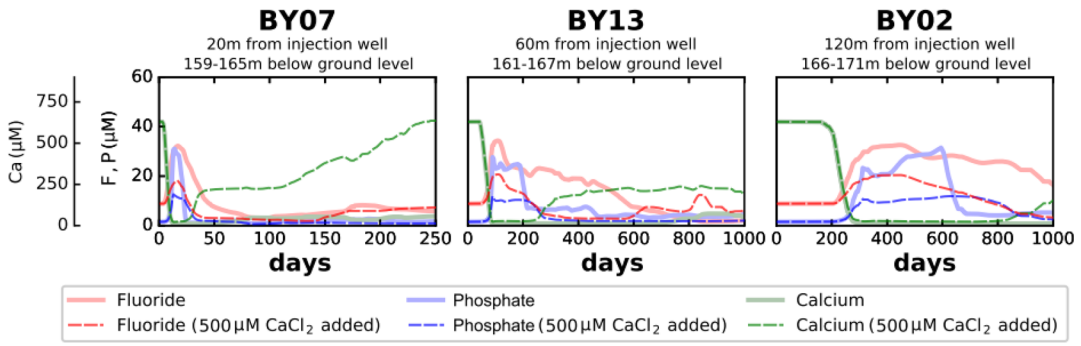

Figure 5. Simulated concentrations of fluoride, phosphate, and calcium for a model scenario (thin dashed lines) in which the injectant was amended with 500 μM $CaCl_2$ in comparison with the corresponding results obtained with the final calibrated model (thick transparent lines).

https://dx.doi.org/10.1021/acs.est.9b06972
Environ. Sci. Technol. XXXX, XXX, XXX−XXX

through the controlled manipulation of the injectant composition. For the present study, we investigated a calcium amendment scenario aimed at reducing fluoride and phosphate release. In this predictive model scenario, 500 μM of calcium chloride ($CaCl_2$) was added to the highly treated recycled water (Table 1). The salt $CaCl_2$ was selected as a possible amendment because it is highly soluble and commonly produced industrially for a variety of uses including as a food additive. The modeling results demonstrate that the addition of 500 μM $CaCl_2$ could lead to a significant reduction in the magnitude (~70−80%) of the fluoride and phosphate pulses (Figure 5). The possible benefits of amending calcium to low ionic strength injectants were also previously shown by Borgnino et al.,[62] who found that calcium amendment could limit fluoride release from FAPs. Nevertheless, the predictive model scenario in this study, which used $CaCl_2$, should be regarded as an illustrative example for demonstrating the usefulness of a process-based modeling approach. The best choice of chemical amendment for mitigating fluoride release, while avoiding potential unintended impacts on the groundwater quality, will require a site-specific assessment that incorporates engineering and cost constraints.[63] Fluoride-bearing apatite minerals, including CFA and FAP, are present in many aquifers worldwide. To prevent geogenic groundwater fluoride contamination by MAR and other water management schemes in these types of aquifers, it is important to avoid the potential of water-sediment disequilibria due to processes affecting dissolved calcium concentrations.

■ ASSOCIATED CONTENT

Supporting Information

The Supporting Information is available free of charge at https://pubs.acs.org/doi/10.1021/acs.est.9b06972.

Additional data collected by complementary experimental work and additional details on the parameters and simulation outputs from the numerical model (PDF)

■ AUTHOR INFORMATION

Corresponding Authors

Jing Sun − *State Key Laboratory of Environmental Geochemistry, Institute of Geochemistry, Chinese Academy of Sciences, Guiyang 550081, P. R. China; School of Earth Sciences, University of Western Australia, Perth, Western Australia 6009, Australia; CSIRO Land and Water, Wembley, Western Australia 6913, Australia;* orcid.org/0000-0002-0129-5184; Phone: (+61) 8 9333 6011; Email: sunjing@mail.gyig.ac.cn; Fax: (+61) 8 9333 6499

Henning Prommer − *School of Earth Sciences, University of Western Australia, Perth, Western Australia 6009, Australia; National Centre for Groundwater Research and Training (NCGRT), Adelaide, South Australia 5001, Australia; CSIRO Land and Water, Wembley, Western Australia 6913, Australia;* orcid.org/0000-0002-8669-8184; Phone: (+61) 8 9333 6272; Email: henning.prommer@csiro.au; Fax: (+61) 8 9333 6499

Authors

David Schafer − *School of Earth Sciences, University of Western Australia, Perth, Western Australia 6009, Australia; National Centre for Groundwater Research and Training (NCGRT), Adelaide, South Australia 5001, Australia*

James Jamieson − *School of Earth Sciences, University of Western Australia, Perth, Western Australia 6009, Australia; CSIRO Land and Water, Wembley, Western Australia 6913, Australia*

Adam J. Siade − *School of Earth Sciences, University of Western Australia, Perth, Western Australia 6009, Australia; National Centre for Groundwater Research and Training (NCGRT), Adelaide, South Australia 5001, Australia; CSIRO Land and Water, Wembley, Western Australia 6913, Australia*

Olivier Atteia − *ENSEGID, EA 4592, Institut Polytechnique de Bordeaux, 33607 Pessac Cedex, France*

Complete contact information is available at: https://pubs.acs.org/10.1021/acs.est.9b06972

Notes

The authors declare no competing financial interest.

■ ACKNOWLEDGMENTS

D.S. was funded through a Robert and Maude Gledden scholarship from the University of Western Australia as well as a top-up scholarship from the National Centre for Groundwater Research and Training (NCGRT) and CSIRO Land and Water. H.P., J.S., and A.J.S. were all partially supported by the Water Corporation of Western Australia ("*Groundwater Replenishment Project—Stages 3 and 4*" and "*Advanced Modelling Methodologies for Groundwater Resource Management and Asset Investment Planning*"), who also provided all required field as well as all required operational data. The PEST++ calibration was conducted on CSIRO's Pearcey high performance computer cluster. We would like to thank Joanne Vanderzalm for her helpful comments on an earlier version of the manuscript.

■ REFERENCES

(1) Newland, P. The development, application and acceptance of environmental and health risk assessment methodology for MAR schemes in South Australia. *Environ. Earth Sci.* **2015**, *73* (12), 7739−7745.

(2) Henzler, A. F.; Greskowiak, J.; Massmann, G. Modeling the fate of organic micropollutants during river bank filtration (Berlin, Germany). *J. Contam. Hydrol.* **2014**, *156*, 78−92.

(3) Fakhreddine, S.; Dittmar, J.; Phipps, D.; Dadakis, J.; Fendorf, S. Geochemical triggers of arsenic mobilization during managed aquifer recharge. *Environ. Sci. Technol.* **2015**, *49* (13), 7802−7809.

(4) Pavelic, P.; Dillon, P. J.; Barry, K. E.; Vanderzalm, J. L.; Correll, R. L.; Rinck-Pfeiffer, S. M. Water quality effects on clogging rates during reclaimed water ASR in a carbonate aquifer. *J. Hydrol.* **2007**, *334* (1−2), 1−16.

(5) Dillon, P.; Stuyfzand, P.; Grischek, T.; Lluria, M.; Pyne, R. D. G.; Jain, R. C.; Bear, J.; Schwarz, J.; Wang, W.; Fernandez, E.et al. Sixty years of global progress in managed aquifer recharge. *Hydrogeol. J.* **2019**, *27*, 1

(6) Hamann, E.; Stuyfzand, P. J.; Greskowiak, J.; Timmer, H.; Massmann, G. The fate of organic micropollutants during long-term/long-distance river bank filtration. *Sci. Total Environ.* **2016**, *545*−*546*, 629−640.

(7) Hiscock, K. M.; Grischek, T. Attenuation of groundwater pollution by bank filtration. *J. Hydrol.* **2002**, *266* (3), 139−144.

(8) Brown, C. J.; Misut, P. E. Aquifer geochemistry at potential aquifer storage and recovery sites in coastal plain aquifers in the New York city area, USA. *Appl. Geochem.* **2010**, *25* (9), 1431−1452.

(9) Descourvieres, C.; Hartog, N.; Patterson, B. M.; Oldham, C.; Prommer, H. Geochemical controls on sediment reactivity and buffering processes in a heterogeneous aquifer. *Appl. Geochem.* **2010**, *25* (2), 261−275.

(10) Vanderzalm, J. L.; Page, D. W.; Barry, K. E.; Dillon, P. J. A comparison of the geochemical response to different managed aquifer recharge operations for injection of urban stormwater in a carbonate aquifer. *Appl. Geochem.* **2010**, *25* (9), 1350−1360.
(11) Wallis, I.; Prommer, H.; Simmons, C. T.; Post, V.; Stuyfzand, P. J. Evaluation of Conceptual and Numerical Models for Arsenic Mobilization and Attenuation during Managed Aquifer Recharge. *Environ. Sci. Technol.* **2010**, *44* (13), 5035−5041.
(12) Wallis, I.; Prommer, H.; Pichler, T.; Post, V.; Norton, S. B.; Annable, M. D.; Simmons, C. T. Process-Based Reactive Transport Model To Quantify Arsenic Mobility during Aquifer Storage and Recovery of Potable Water. *Environ. Sci. Technol.* **2011**, *45* (16), 6924−6931.
(13) Treumann, S.; Torkzaban, S.; Bradford, S. A.; Visalakshan, R. M.; Page, D. An explanation for differences in the process of colloid adsorption in batch and column studies. *J. Contam. Hydrol.* **2014**, *164* (0), 219−229.
(14) Jones, G. W.; Pichler, T. Relationship between Pyrite Stability and Arsenic Mobility During Aquifer Storage and Recovery in Southwest Central Florida. *Environ. Sci. Technol.* **2007**, *41* (3), 723−730.
(15) McNab, W. W., Jr; Singleton, M. J.; Moran, J. E.; Esser, B. K. Ion exchange and trace element surface complexation reactions associated with applied recharge of low-TDS water in the San Joaquin Valley, California. *Appl. Geochem.* **2009**, *24* (1), 129−137.
(16) Seibert, S.; Atteia, O.; Ursula Salmon, S.; Siade, A.; Douglas, G.; Prommer, H. Identification and quantification of redox and pH buffering processes in a heterogeneous, low carbonate aquifer during managed aquifer recharge. *Water Resour. Res.* **2016**, *52* (5), 4003−4025.
(17) Antoniou, E. A.; van Breukelen, B. M.; Putters, B.; Stuyfzand, P. J. Hydrogeochemical patterns, processes and mass transfers during aquifer storage and recovery (ASR) in an anoxic sandy aquifer. *Appl. Geochem.* **2012**, *27* (12), 2435−2452.
(18) Rathi, B.; Siade, A. J.; Donn, M. J.; Helm, L.; Morris, R.; Davis, J. A.; Berg, M.; Prommer, H. Multiscale Characterization and Quantification of Arsenic Mobilization and Attenuation During Injection of Treated Coal Seam Gas Coproduced Water into Deep Aquifers. *Water Resour. Res.* **2017**, *53* (12), 10779−10801.
(19) Prommer, H.; Sun, J.; Helm, L.; Rathi, B.; Siade, A. J.; Morris, R. Deoxygenation Prevents Arsenic Mobilization during Deepwell Injection into Sulfide-Bearing Aquifers. *Environ. Sci. Technol.* **2018**, *52* (23), 13801−13810.
(20) WHO. Guidelines for Drinking-Water Quality: Incorporating the First Addendum, 4th ed.; World Health Organization: 2017; p 541.
(21) Jha, S. K.; Singh, R. K.; Damodaran, T.; Mishra, V. K.; Sharma, D. K.; Rai, D. Fluoride in Groundwater: Toxicological Exposure and Remedies. *J. Toxicol. Environ. Health, Part B* **2013**, *16* (1), 52−66.
(22) Vithanage, M.; Bhattacharya, P. Fluoride in the environment: sources, distribution and defluoridation. *Environ. Chem. Lett.* **2015**, *13* (2), 131−147.
(23) Fantong, W. Y.; Satake, H.; Ayonghe, S. N.; Suh, E. C.; Adelana, S. M. A.; Fantong, E. B. S.; Banseka, H. S.; Gwanfogbe, C. D.; Woincham, L. N.; Uehara, Y.; Zhang, J. Geochemical provenance and spatial distribution of fluoride in groundwater of Mayo Tsanaga River Basin, Far North Region, Cameroon: implications for incidence of fluorosis and optimal consumption dose. *Environ. Geochem. Health* **2010**, *32* (2), 147−163.
(24) Gaus, I.; Shand, P.; Gale, I. N.; Williams, A. T.; Eastwood, J. C. Geochemical modelling of fluoride concentration changes during Aquifer Storage and Recovery (ASR) in the Chalk aquifer in Wessex, England. *Q. J. Eng. Geol. Hydrogeol.* **2002**, *35* (2), 203−208.
(25) Stone, M. L.; Garrett, J. D.; Poulton, B. C.; Ziegler, A. C. *Effects of Aquifer Storage and Recovery Activities on Water Quality in the Little Arkansas River and Equus Beds Aquifer, South-Central Kansas, 2011−14*; 2328−0328; US Geological Survey: 2016.
(26) Brindha, K.; Jagadeshan, G.; Kalpana, L.; Elango, L. Fluoride in weathered rock aquifers of southern India: Managed Aquifer Recharge for mitigation. *Environ. Sci. Pollut. Res.* **2016**, *23* (9), 8302−8316.
(27) Schafer, D.; Donn, M.; Atteia, O.; Sun, J.; Macrae, C.; Raven, M.; Pejcic, B.; Prommer, H. Fluoride and phosphate release from carbonate-rich fluorapatite during managed aquifer recharge. *J. Hydrol.* **2018**, *562*, 809−820.
(28) Hughes, J. M. The many facets of apatite. *Am. Mineral.* **2015**, *100* (5−6), 1033−1039.
(29) Hughes, J. M.; Rakovan, J. F. Structurally Robust, Chemically Diverse: Apatite and Apatite Supergroup Minerals. *Elements* **2015**, *11* (3), 165−170.
(30) Chaïrat, C.; Oelkers, E. H.; Schott, J.; Lartigue, J.-E. Fluorapatite surface composition in aqueous solution deduced from potentiometric, electrokinetic, and solubility measurements, and spectroscopic observations. *Geochim. Cosmochim. Acta* **2007**, *71* (24), 5888−5900.
(31) Chaïrat, C.; Schott, J.; Oelkers, E. H.; Lartigue, J.-E.; Harouiya, N. Kinetics and mechanism of natural fluorapatite dissolution at 25°C and pH from 3 to 12. *Geochim. Cosmochim. Acta* **2007**, *71* (24), 5901−5912.
(32) Christoffersen, J.; Christoffersen, M. R.; Johansen, T. Some new aspects of surface nucleation applied to the growth and dissolution of fluorapatite and hydroxyapatite. *J. Cryst. Growth* **1996**, *163* (3), 304−310.
(33) Tribble, J. S.; Arvidson, R. S.; Lane, M.; Mackenzie, F. T. Crystal chemistry, and thermodynamic and kinetic properties of calcite, dolomite, apatite, and biogenic silica: applications to petrologic problems. *Sediment. Geol.* **1995**, *95* (1−2), 11−37.
(34) Dorozhkin, S. V. Surface Reactions of Apatite Dissolution. *J. Colloid Interface Sci.* **1997**, *191* (2), 489−497.
(35) Dorozhkin, S. V. Acidic dissolution mechanism of natural fluorapatite. II. Nanolevel of investigations. *J. Cryst. Growth* **1997**, *182* (1−2), 133−140.
(36) Jahnke, R. A. The synthesis and solubility of carbonate fluorapatite. *Am. J. Sci.* **1984**, *284* (1), 58−78.
(37) Guidry, M. W.; Mackenzie, F. T. Experimental study of igneous and sedimentary apatite dissolution: Control of pH, distance from equilibrium, and temperature on dissolution rates. *Geochim. Cosmochim. Acta* **2003**, *67* (16), 2949−2963.
(38) Perrone, J.; Fourest, B.; Giffaut, E. Surface Characterization of Synthetic and Mineral Carbonate Fluoroapatites. *J. Colloid Interface Sci.* **2002**, *249* (2), 441−452.
(39) Zack, A. L. *Geochemistry of Fluoride in the Black Creek Aquifer System of Horry and Georgetown Counties, South Carolina—and its Physiological Implications*; Water-supply paper 2067; USGS: 1980.
(40) Edmunds, W. M.; Smedley, P. Fluoride in Natural Waters. In *Essentials of Medical Geology*; Selinus, O., Ed.; Springer: Netherlands, 2013; pp 311−336.
(41) Ganot, Y.; Holtzman, R.; Weisbrod, N.; Russak, A.; Katz, Y.; Kurtzman, D. Geochemical processes during managed aquifer recharge with desalinated seawater. *Water Resour. Res.* **2018**, *54* (2), 978−994.
(42) Stuyfzand, P.; Smidt, E.; Zuurbier, K.; Hartog, N.; Dawoud, M. Observations and prediction of recovered quality of desalinated seawater in the strategic ASR project in Liwa, Abu Dhabi. *Water* **2017**, *9* (3), 177.
(43) Vandenbohede, A.; Wallis, I.; Van Houtte, E.; Van Ranst, E. Hydrogeochemical transport modeling of the infiltration of tertiary treated wastewater in a dune area, Belgium. *Hydrogeol. J.* **2013**, *21* (6), 1307−1321.
(44) Prommer, H.; Sun, J.; Kocar, B. D. Using Reactive Transport Models to Quantify and Predict Groundwater Quality. *Elements* **2019**, *15* (2), 87−92.
(45) Water Corporation. Site Characterization Report—Groundwater Replenishment Trial. In Perth, Australia: 2009; p 163.
(46) Leyland, L. *Hydrogeology of the Leederville Aquifer, Central Perth Basin, Western Australia*; University of Western Australia, 2011.

https://dx.doi.org/10.1021/acs.est.9b06972
Environ. Sci. Technol. XXXX, XXX, XXX−XXX

(47) Descourvieres, C.; Douglas, G.; Leyland, L.; Hartog, N.; Prommer, H. Geochemical reconstruction of the provenance, weathering and deposition of detrital-dominated sediments in the Perth Basin: The Cretaceous Leederville Formation, south-west Australia. *Sediment. Geol.* **2011**, *236* (1−2), 62−76.
(48) Dickson, A. G.; Goyet, C. *Handbook of Methods for the Analysis of the Various Parameters of the Carbon Dioxide System in Sea Water*, Version 2; Oak Ridge National Lab.: TN, 1994.
(49) Seibert, S.; Prommer, H.; Siade, A.; Harris, B.; Trefry, M.; Martin, M. Heat and mass transport during a groundwater replenishment trial in a highly heterogeneous aquifer. *Water Resour. Res.* **2014**, *50* (12), 9463−9483.
(50) Harbaugh, A. W. *MODFLOW-2005, The U.S. Geological Survey Modular Ground-Water Model—the Ground-Water Flow Process*; U.S. Geological Survey Techniques and Methods 6-A16; U.S. Department of the Interior, U.S. Geological Survey: 2005; p 253.
(51) Prommer, H.; Barry, D.; Zheng, C. MODFLOW/ MT3DMS − based reactive 1076 multicomponent transport modelling. *Groundwater* **2003**, *41* (2), 247−257.
(52) McClellan, G. H. Mineralogy of carbonate fluorapatites. *J. Geol. Soc.* **1980**, *137* (6), 675−681.
(53) Wagman, D. D.; Evans, W. H.; Parker, V. B.; Schumm, R. H.; Hallow, I.; Bailey, S. S.; Churney, K. L.; Nuttall, R. L. NBS tables of chemical thermodynamic properties. *J. Phys. Chem.* **1982**, *Chem. Ref. Data 111*(Suppl. 1).
(54) Karamalidis, A. K.; Dzombak, D. A. *Surface Complexation Modeling—Gibbsite*; John Wiley & Sons, Inc.: New York, 2010; p 294.
(55) Blanc, P. *Thermoddem—Thermochemical and Mineralogical Tables for Geochemical Modeling*. In Minières), Orléans, France, 2018.
(56) Welter, D. E.; White, J. T.; Hunt, R. J.; Doherty, J. E. *Approaches in Highly Parameterized Inversion—PEST++ Version 3, A Parameter ESTimation and Uncertainty Analysis Software Suite Optimized for Large Environmental Models*; 2328−7055; US Geological Survey: 2015.
(57) Sun, J.; Prommer, H.; Siade, A. J.; Chillrud, S. N.; Mailloux, B. J.; Bostick, B. C. Model-Based Analysis of Arsenic Immobilization via Iron Mineral Transformation under Advective Flows. *Environ. Sci. Technol.* **2018**, *52* (16), 9243−9253.
(58) Descourvieres, C. *Quantifying Water Quality Changes during Managed Aquifer Recharge in a Physically and Chemically Heterogeneous Aquifer*; The University of Western Australia: Perth, WA, 2011.
(59) Andersson, K. O.; Tighe, M. K.; Guppy, C. N.; Milham, P. J.; McLaren, T. I.; Schefe, C. R.; Lombi, E. XANES Demonstrates the Release of Calcium Phosphates from Alkaline Vertisols to Moderately Acidified Solution. *Environ. Sci. Technol.* **2016**, *50* (8), 4229−4237.
(60) Sun, J.; Quicksall, A. N.; Chillrud, S. N.; Mailloux, B. J.; Bostick, B. C. Arsenic mobilization from sediments in microcosms under sulfate reduction. *Chemosphere* **2016**, *153*, 254−261.
(61) Edzwald, J. K.; Toensing, D. C.; Leung, M. C.-Y. Phosphate adsorption reactions with clay minerals. *Environ. Sci. Technol.* **1976**, *10* (5), 485−490.
(62) Borgnino, L.; Garcia, M. G.; Bia, G.; Stupar, Y. V.; Le Coustumer, P.; Depetris, P. J. Mechanisms of fluoride release in sediments of Argentina's central region. *Sci. Total Environ.* **2013**, *443* (0), 245−255.
(63) Birnhack, L.; Voutchkov, N.; Lahav, O. Fundamental chemistry and engineering aspects of post-treatment processes for desalinated water—a review. *Desalination* **2011**, *273* (1), 6−22.
(64) Parkhurst, D. L. *PHREEQC (Version 3)—A Computer Program for Speciation, Batch-Reaction, One-Dimensional Transport, and Inverse Geochemical Calculations*; In US Geological Survey: 2015.
(65) Doherty, J. *PEST Model-Independent Parameter Estimation User Manual—User Manual Part I: PEST, SENSAN and Global Optimisers*, 7th ed.; Watermark Numerical Computing: www.pesthomepage.org/Downloads.php, 2018.

https://dx.doi.org/10.1021/acs.est.9b06972
Environ. Sci. Technol. XXXX, XXX, XXX−XXX